Isotope effects on the charge transfer into the $n = 1$, 2, and 3 shells of He^{2+} in collisions with H, D, and T

N. Stolterfoht,[1,2,*] R. Cabrera-Trujillo,[1,3] P. S. Krstić,[4] R. Hoekstra,[5] Y. Öhrn,[1] E. Deumens,[1] and J. R. Sabin[1]

[1]*Quantum Theory Project, Departments of Physics and Chemistry, University of Florida, Gainesville, Florida 32611-8435, USA*

[2]*Helmholtz-Zentrum Berlin, Glienickerstraße 100, D-14109 Berlin, Germany*

[3]*Instituto de Ciencias Físicas, Universidad Nacional Autónoma de México, Apartado Postal 48-3, Cuernavaca, Morelos 62251, México*

[4]*Physics Division, Oak Ridge National Laboratory, Oak Ridge, Tennessee 37831, USA*

[5]*KVI Atomic Physics, University of Groningen, NL-9747 AA Groningen, The Netherlands*

(Received 30 November 2009; published 19 May 2010)

Processes for charge transfer into He^{2+} colliding with the atomic isotopes hydrogen (H), deuterium (D), and tritium (T) are theoretically studied at collision energies as low as 30 eV/amu. Probabilities and cross sections for electron capture into different shells of the projectile are calculated using an ab initio approach which solves the time-dependent Schrödinger equation. The results are interpreted in terms of radial and rotational couplings between molecular orbitals. The probabilities exhibit strong Stueckelberg oscillations for charge transfer into shells with the principal quantum numbers $n = 2$ and 3 due to radial coupling mechanisms in specific ranges of the impact parameter. The total cross sections for charge transfer, evaluated for a given shell, differ by orders of magnitude, as different isotopes are used in the collisions. The isotope effect increases significantly for decreasing $n = 3$, 2, and 1. This finding is attributed to the influence of the rotational coupling mechanism, which is strongly affected by the distance of closest approach between the collision partners.

DOI: 10.1103/PhysRevA.81.052704 PACS number(s): 34.50.Fa, 32.80.Fb

I. INTRODUCTION

Charge transfer processes in $He^{2+} + H$ collisions [1] have received outstanding attention in several fields of basic research and technological applications. Atomic hydrogen and helium are the most abundant elements in both astrophysical and terrestrial fusion plasmas. After protons, the main constituents of the solar wind are He^{2+} ions, which contribute up to a few percent. When these ions interact with cometary atmospheres, charge exchange into excited states generates VUV emission, which can be used as a diagnostics tool [2,3]. In the outer parts of the atmosphere the main reaction partner is atomic hydrogen [4]. Here interaction energies are typically in the range of 50–2000 eV/amu.

In terrestrial fusion plasmas, helium ash is the main product of the D-T fusion reaction and constitutes an important ingredient in the dynamics of maintaining the plasma. α particles, which have been slowed down by collisions and reach the cooler outer plasma boundary, can recombine with an electron along various pathways into excited He^{+} states and thus contribute to radiative cooling [5,6]. In the boundary layer of the plasma, a significant fraction of neutral H atoms, which are being desorbed and sputtered from the walls, is available for charge exchange reactions with α particles. The latter helps to accommodate the large power flux from the plasma core onto the surrounding walls and the divertor target plates [7].

Because of its importance, the collision system $He^{2+} + H$ has been studied extensively in theoretical and experimental work. Several experiments have been performed to study charge exchange processes in such collisions. (For references see [8] and [9]). However, experiments on charge transfer in $He^{2+} + H$ collisions require a great deal of technological effort. Specific techniques are necessary to produce a target of atomic hydrogen with a sufficiently high density and atomic purity. Consequently, experiments are difficult to perform at energies lower than about 300 eV/amu [9,10]. Below this value the cross sections for charge exchange are too small for the current experimental techniques. Hence, at lower energies the plasma physics community has to rely exclusively on theoretical results.

For theorists, the $He^{2+} + H$ system is of great interest, since it is the simplest asymmetric ion-atom collision system carrying a single electron. As a fundamental three-particle problem, $He^{2+} + H$ is the benchmark system of charge transfer theory [11]. It has served as a challenge and reference for several groups that apply quantum mechanics for the treatment of atomic collisions. Hence, numerous theoretical approaches have been applied to study $He^{2+} + H$ collisions. (References to the theoretical work are given in [7,8,12], and [13]). In these previous studies excellent agreement among the different calculated cross sections is achieved at energies above 1000 eV/amu.

At lower energies, significant differences occur between the previous theoretical approaches. However, recent theoretical studies applying hyperspherical coordinates and reaction coordinates of Le *et al.* [14] and the hidden crossing coupled-channel approach of Krstić [8] have yielded converging cross sections. Hence, for collision energies from 10 to 400 eV/amu, these calculations can be considered as a standard for charge transfer cross sections in $He^{2+} + H$ collisions [7]. Most recent investigations [13,15] were found to be in good agreement with these standard results.

Previous studies have shown that the probability for charge transfer in $He^{2+} + H$ collisions exhibits sinusoidal oscillations when plotted as a function of the impact parameter [8,14,15]. Such oscillations were discovered by Stueckelberg [16] in the early 1930s. They are produced by coherent contributions from two localized transition regions, similarly to Young's

*nico@stolterfoht.com

well-known two-slit experiment [17]. In $He^{2+} + H$ collisions, the charge transfer into the $n = 2$ shell of the projectile presents an outstanding example of two-component interference in a system of atomic dimensions. Similar interferences have recently been found for capture into the $n = 3$ shell in the same collision system [18].

In view of the extensive studies of $He^{2+} + H$ collisions, one would expect that the corresponding collisions with the isotopes D and T had received similar attention. The corresponding collision systems are of considerable interest for modeling the plasma in a fusion reactor. In the boundary layer of the plasma a significant fraction of neutral D and T atoms, which are being desorbed and sputtered from the walls, is available for charge exchange reactions with α particles. However, to the best of our knowledge, investigation of He^{2+} impact on D and T has been performed only in our recent theoretical study [15], referred to as I in the following. It was found that at collision energies of less than 100 eV/amu, the capture cross sections for the target atoms D and T exceed those for H by orders of magnitude. This finding is attributed to differences in the trajectories of the colliding particles involving different isotopes as target atoms. Trajectory effects on excitation and capture processes have been studied before [1], however, their importance for isotope effects has only recently been observed [15].

In the present work, we extended our theoretical study carried out in I. As before we used the theoretical approach known as electron nuclear dynamics (END) [19], which explicitly solves the time-dependent Schrödinger equation. In comparison with I, the calculations were redone using a larger basis set and extended to projectile energies as low as 30 eV/amu. The important aspect of the present work is the investigation of isotope effects for charge transfer into individual shells of the projectile. Cross sections for charge transfer into shells with $n = 1$, 2, and 3 were determined. The corresponding isotope effects were found to be significantly different for the different shells.

II. THEORETICAL METHOD

The END theory is an explicitly time-dependent, direct method that takes into account the nonadiabatic coupling between the nuclear and the electronic degrees of freedom. For description of electronic motion a quantal atomic orbital expansion method is used, while internuclear motion is described classically following the instantaneous coupling with the electrons. The theoretical predictions of the END approach agree well with measured differential and integral cross sections for ion-atom and ion-molecule collisions. Since theory has been described in detail in several previous works (see, e.g., [18–22], and references therein), here we provide a brief overview of the main features of the theory.

The equations that govern the time evolution of the system are derived using a time-dependent variational principle and form a set of coupled first-order differential equations. Let $\mathbf{R}_k$ and $\mathbf{P}_k$ be the positions and momenta of the nucleus k. For our one-electron system, the wave function $\psi_h = u_h + \sum_p u_p z_{ph}$ is the linear combinations of atomic orbitals $u_j, j = 1, \ldots, K$. The complex expansion coefficients z_{ph} of the orbitals ψ_j in terms of the basis orbitals u_j are then the dynamic variables of the theory. These atomic orbitals include electron translation factors to ensure Galilean invariance and a proper account of charge transfer [14]. Application of the time-dependent variational principle to the action produced by the quantum mechanical Lagrangian $L = \langle\psi|i\hbar\partial/\partial t - H|\psi\rangle/\langle\psi|\psi\rangle$, with H the system Hamiltonian combined with the Euler-Lagrange equations produces the equation of motion of the dynamic variables of the system. These equations are described in detail in the review paper [19] and are solved by numerical integration in time.

The atomic wave function is described as a linear combination of Gaussian functions centered on the nuclei. The Gaussian functions have the form

$$\varphi_i(\mathbf{r}) = \sum_j d_{ij}(x - R_x)^n (y - R_y)^m (z - R_z)^l e^{-\alpha_{ij}(\mathbf{r}-\mathbf{R})^2} \qquad (1)$$

and are centered on the average nuclear positions $\mathbf{R}_k$ with exponents α_{ij} and contraction coefficient d_{ij}. Here n, m, and l are integer numbers. From this basis set, a linear combination of atomic orbitals is formed, which are then used to construct the initial molecular orbitals of the system. In the present calculations, the electronic states centered at H and He are expressed in terms of the correlation-consistent, polarized-valence double- and triple-Z basis sets aug-cc-pVDZ and aug-cc-pVTZ, respectively, from Dunning [23].

For the hydrogen atom we obtain a self-consistent field ground state for the $1s^1$ configuration by means of a [*5s2p/3s2p*] basis set, augmented by two s and one p even-tempered diffuse orbitals to allow for low-lying excitations of the target. For the He^{2+} projectile we used a [*7s3p2d/4s3p2d*] basis set, augmented by two s, three p, and two d even-tempered diffuse orbitals to reproduce the low-excited states. We note that with the inclusion of the two d orbitals, the present basis is enlarged in comparison with our previous studies [15,18]. Therefore, small deviations occur between the present results and those presented in I.

The total ground-state energies obtained for these atoms when a single electron is attached to them are $E(\mathrm{H}) = -0.499339$ a.u. and $E(\mathrm{He}^+) = -1.999120$ a.u. For hydrogen we get a good description of the $n = 1$ and 2 shell energies, as well as the $n = 1$, 2, and 3 shells of the He^+ ion. These bases yield the binding energies for $n = 1$, 2, and 3 within 1% of their exact values. Also, the molecular potential energies (shown in Fig. 1) were calculated with an agreement of 1% with the exact results (see, e.g., [8]). With the present basis set including diffuse orbitals, we obtain 13 pseudocontinuum states which describe the low region of the ionization channel.

The grid for the impact parameters b was divided into two regions: (i) close collisions, for which b is varied in steps of 0.05 a.u. from 0 to 2 a.u.; and (ii) collisions for which b runs in steps of 0.1 a.u. from 2 to 6 a.u. and in steps of 0.2 a.u. from 6 to 10 a.u. The target atom was placed at the origin of a Cartesian coordinate system and the projectile was initially located far away from the origin. The trajectory was begun with the He^{2+} projectile moving parallel to the z axis with a displacement by an amount b from it in the x direction. This movement along the z axis continued until the projectile was deflected by the interaction with the target atom. The favorable feature of the END method is that the trajectories of the heavy particles

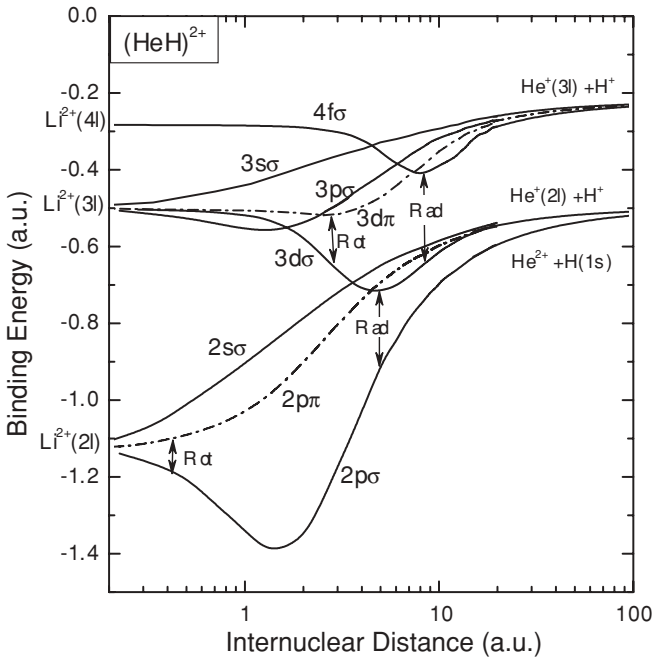

FIG. 1. Adiabatic electronic energies of the molecular orbitals for the system $(HeH)^{2+}$. The arrows labeled "Rot" and "Rad" denote the approximate localizations of the rotational and radial couplings, respectively.

are governed by a scattering potential that is evolving in accordance with the dynamics of the electrons. The trajectories were allowed to run past the target until there was no further change in the electronic charges on the projectile or target.

As the state evolves from the initial state i, one obtains the electronic wave function $\psi_i(t)$ at time t. The electron capture probability is obtained by projecting the asymptotic wave function $\psi_i(\infty)$ onto a particular final electronic state ψ_f of the projectile, expressed in terms of the projectile basis set. Thus, the probability of finding the electron in that final state is given by $P_f(b) = |\langle\psi_f|\psi_i(\infty)\rangle|^2$, where ψ_f is the stationary electronic state we are interested in, for example, the $2p$ state of the He^+ ion projectile. In our notation we obtain $P_f(b) = \mathbf{z}_f^\dagger \mathbf{S} \mathbf{z}_i$, where $\mathbf{z}_f^\dagger$ is the complex transpose vector array of the molecular coefficients of the final state we want to project in, $\mathbf{z}_i$ is the evolved vector array of the molecular coefficients from the initial state i, and $\mathbf{S}$ is the overlap matrix determined from the basis set.

To comment on the precision of the capture probabilities, we note that at higher energies the present results may be influenced by the fact that ionization is not fully treated within the END approach. Therefore, we generally limited our calculations at energies lower than 1 keV/amu, where ionization is expected to be negligible. At lower energies, where the capture probability becomes small, the results depend sensitively on small changes in couplings and deflections. It should be recalled that the particle trajectories are determined with a high precision, since the scattering potential is based on the dynamics of the nucleus-electron interaction. However, the choice of the basis influences the charge exchange probabilities. We tested various sets of basis states to make sure that convergence problems were minimized. As shown in the following sections, the END results agree well with the cross sections recommended previously [7].

III. GENERAL CONSIDERATIONS

As outlined in the previous section, the results of the present work are obtained using numerical methods, which yield only limited information about the coupling mechanisms. To interpret details of the calculated charge transfer probabilities and cross sections, it is useful to consider a few general features of the present collision systems. In particular, at low collision velocities nonadiabatic transitions between quasimolecular states play an important role. Hence, in the following we give a brief overview of the molecular orbitals involved in the $He^{2+} + H$ system. More information about the electron transfer mechanisms is given in the detailed works by Grozdanov and Solov'ev [24] and Krstić and Janev [25]. In addition, we discuss the kinematics of the collision systems by analyzing the projectile scattering angle as a function of the impact parameter. This is done to obtain information about heavy particle trajectories which govern the isotope effects studied in this work.

A. Coupling of molecular orbitals

In slow collisions, charge transfer can be interpreted in terms of coupling of adiabatic potential energy curves as shown in Fig. 1. As is common practice, these molecular orbitals are specified by the spherical quantum numbers of the united atom limit. In the $He^{2+} + H$ system, the molecular orbital $2p\sigma$ plays the role of the incident channel that initially carries the electron. In the limit of small velocities ($v \to 0$) the electron transition dynamics is localized to narrow coupling regions in the internuclear distance R, where strong nonadiabatic couplings of the adiabatic quasimolecular states take place. In the coupling regions the radial potential barrier between the two ionic centers decreases enough to allow the electron wave function to tunnel through and eventually to expand over it, changing its character from atomic to molecular. The internuclear distance at which the maximum coupling occurs is referred to as coupling radius.

The abrupt change of the electronic wave function is associated with a localized peak in the radial derivative $\partial/\partial R$, that is, in the radial nonadiabatic matrix element of the two relevant adjacent adiabatic states of the same angular symmetry ($\Delta m = 0$). Furthermore, due to the sudden change of the direction of the internuclear axis at the closest distances of the colliding particles, so-called rotational coupling emerges between the states of different angular symmetry ($\Delta m = \pm 1$). This is dependent on the rotation of the internuclear axis and, thus, characterized by the angular derivative $\partial/\partial\theta$ and its relevant matrix element between the coupled adiabatic states.

At large internuclear distances near 6 a.u. the charge transfer into the $n = 2$ shell is produced by the radial coupling between the incident orbital $2p\sigma$ and the orbital $3d\sigma$ as shown in Fig. 1 [24,25]. A further contribution originates from the rotational coupling between the $2p\sigma$ and the $2p\pi$ orbitals at a small internuclear distance, less than 1 a.u. [26,27]. Radial coupling dominates at collision energies higher than 500 eV/amu and its contribution decreases nearly exponentially with decreasing energy [28]. While the radial coupling loses significance, the

rotational coupling gains importance at lower energies, in this case giving rise to significant capture cross sections around 100 eV/amu. At energies below 40 eV/amu the significance of the rotational coupling diminishes and the radial coupling regains the dominance [8].

B. Isotope effects on the particle trajectories

To obtain information on the particle trajectories we consider the kinetic energy E_p of the incident projectile in the laboratory frame and the corresponding center-of-mass energy $E_p^{\text{c.m.}}$ of the collision system, which are defined as

$$E_p = \tfrac{1}{2} M_1 v_i^2 \quad \text{and} \quad E_p^{\text{c.m.}} = \tfrac{1}{2}\mu v_i^2, \tag{2}$$

where $\mu = M_1 M_2/(M_1 + M_2)$ is the reduced mass obtained from the masses M_1 and M_2 of the projectile and target, respectively. Since the target atom is initially at rest, the incident velocity of the projectile v_i is equal to the relative velocity of the collision partners. The results of the present work are given as a function of the reduced laboratory energy $\varepsilon_p = E_p/M_1 = v_i^2/2$, which is a measure of the incident velocity. For simplicity, the quantity ε_p is also referred to as projectile energy or impact energy.

In Fig. 2 we show the scattering angle for He^{2+} as a function of the impact parameter for collisions with H and T for two impact energies, 50 and 10 keV/amu. We recall that the specific feature of the END method is that the trajectories of the heavy particles are governed by a scattering potential that is evolving in accordance with the dynamics of the electron. Due to the effect of the target electron, one observes two impact-parameter regions, wherein the scattering angle has different signs. In the repulsive region, for which $b < 4$ a.u., the projectile penetrates the electronic cloud and "sees" the repulsive nuclei. In the attractive region for $b > 4$ a.u. the projectile is attracted by the electronic cloud and shows negative scattering angles. The latter effect is more pronounced at low collision energies, showing a proper description of the scattering potential. It is evident that a pure Coulomb potential cannot reproduce the negative scattering angles.

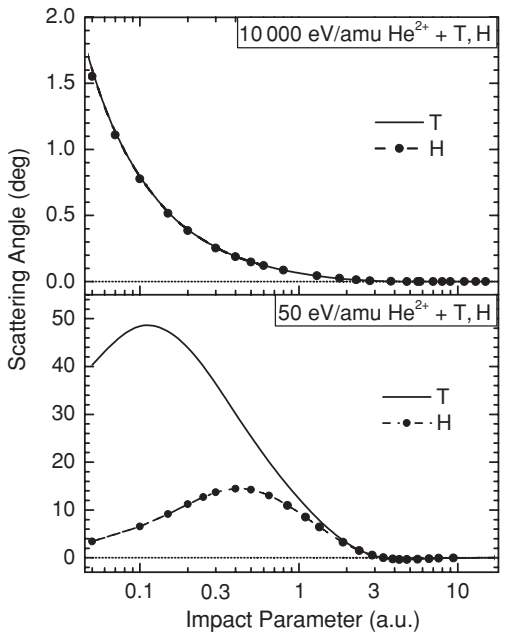

FIG. 2. Scattering angle of the projectile as a function of the impact parameter for the target atoms hydrogen (H) and tritium (T). Impact energies are 10 and 50 eV/amu as indicated.

The primary results of the present data is the isotope effect on the scattering angle, which is found to be significantly different for the two energies. At the high collision energies shown in Fig. 2(a), the scattering angle is less than 2° when He^{2+} collides with both H and T. Thus, the straight trajectory approximation holds for high energies, as expected. The difference between the scattering angle for H and that for T is less than 1% for small impact parameters, so that no noticeable isotope effect is present at high collision energies.

However, as shown in Fig. 2(b) isotopic effects for He^{2+} colliding with H and T can be observed at 50 eV/amu. For both H and T targets, the largest scattering angle occurs for impact parameters $b < 1$ a.u., where we expect that the rotational coupling is dominant. The significant mass ratio of 3 for the two targets plays an important role for the scattering angle. The maximum of the scattering angle is ~3 times higher for T than for H, that is, ~50° for T and ~16° for H. Also, the location of the maximum for T occurs at a distance a factor of 3 smaller than that for H, that is, $b_{\max} \approx 0.13$ a.u. for T and $b_{\max} \approx 0.4$ a.u. for H, thus, showing a larger scattering angle for T than for H. From this we infer a larger rotation during the collision for He^{2+} when impinging on T than when impinging on H at small impact parameters.

The differences in the scattering angle for the isotopes are produced by differences in the trajectories of the heavy particles. Because of its smaller mass, the H atom is recoiled more easily by the repulsive interaction with the incident projectile than the heavier T atom. Therefore, the distance of closest approach in the collision is significantly larger for H than for T. For the extreme impact parameters close to zero, the distance of closest approach can readily be estimated from

$$R_{\min} = \frac{Z_1 Z_2}{E_p^{\text{c.m.}}}, \tag{3}$$

where Z_1 and Z_2 are the (screened) nuclear charges of the collision partners. As the reduced mass and, thus, the center-of-mass energy of H and T differ by more than a factor of 2, the distance of closest approach varies considerably for the present isotopes. In the following sections it is shown that the differences in the particle trajectories are the reason for the isotope effects studied here.

We emphasize that it is crucial for the size of the isotopic effects to take into account at least classical internuclear trajectories, calculated from the realistic internuclear potential as used in this work. Ideally, a quantum approach should be applied to the internuclear motion [8] at lowest energies rather than a classical treatment, which was chosen in the present END version. The methods in Refs. [24] and [25], involving an assumption of a straight-line trajectory, cannot reproduce the rotational transition-dominated isotopic effect treated in this work. Even the Coulomb trajectory approximation, used in an estimation of rotational couplings [27], would not describe accurately either rotational transitions or isotopic effects at the low end of the considered energy range [29].

IV. CHARGE TRANSFER PROBABILITIES

In the following we present probabilities of charge transfer into different shells of He^{2+}. The discussion of the probabilities is based on the couplings of the molecular orbitals as shown in Fig. 1. We start with charge transfer into the $n = 2$ shell, since most information is available for this shell [8,18] so that its discussion is unambiguous. For the $n = 3$ shell the interpretation is less secure, although still based on solid ground, whereas the discussion of the $n = 1$ shell contains suggestions which may need further consideration.

A. Transfer into the $n = 2$ shell

Figure 3 shows the calculated probability $P_2(b)$ for charge transfer into the $n = 2$ shell of He^{2+} upon collision with H and T. The probabilities for the projectile energies 50, 100, and 250 eV/amu are given as a function of the impact parameter b. The inner and outer ranges of the impact parameter are separated by the vertical lines drawn near 1 a.u. Although somewhat arbitrary, the separation into two impact parameter ranges is useful, as it allows for a separate view of the contributions from the rotational and radial coupling mechanisms. It is recalled that the internuclear distances for the two processes differ by an order of magnitude. The contribution of the rotational coupling occurs at small impact parameters, below $b = 1$ a.u., whereas that of the radial coupling is important from $b = 1$ a.u. upward.

In the inner region the probabilities $P_2(b)$ show distinct maxima at $b \approx 0.2$ a.u. which originate from transitions due to $2p\sigma$-$2p\pi$ rotational coupling. In the outer region the probabilities $P_2(b)$ exhibit oscillatory structures, which are due to the Stueckelberg interferences [16] discussed in detail previously [18]. Figure 3 shows that, apart from a small phase shift, the charge transfer probabilities for the H and T atoms agree within the outer region (dominated by radial coupling). The phase shifts are due to isotope effects that produce certain differences in the particle trajectories and relative projectile-target velocities.

As shown in Fig. 3 large isotope effects are observed within the inner region, which is governed by rotational coupling. This provides clear evidence that the rotational coupling is mainly responsible for the isotope effects on the charge transfer. The difference between the results for H and T increases strongly with decreasing energy. At 50 eV/amu the probabilities for the two isotopes differ by about 3 orders of magnitude. We return to this finding in the discussion of total cross sections.

B. Transfer into $n = 3$ and 1 shells

Figure 4 shows the calculations of the probability $P_3(b)$ for charge transfer into the $n = 3$ shell of He^{2+} upon collision with H and T for impact energies of 50, 100, and 250 eV/amu. Although numerous orbitals may be involved in transitions to higher orbitals, there are only a few pathways along the potential curves resulting in capture into the $n = 3$ shell (Fig. 1).

It is important to keep in mind that the charge transfer into the $n = 3$ shell is preceded by transitions into the $n = 2$ shell due to $2p\sigma$-$3d\sigma$ radial and $2p\sigma$-$2p\pi$ rotational couplings. Figure 4 shows that the capture probabilities exhibit distinct peaks at $b \approx 0.2$ a.u., which are likely to be produced by transitions due to the $2p\sigma$-$2p\pi$ rotational coupling mechanism, followed by radial coupling of the $2p\pi$ and the $3d\pi$

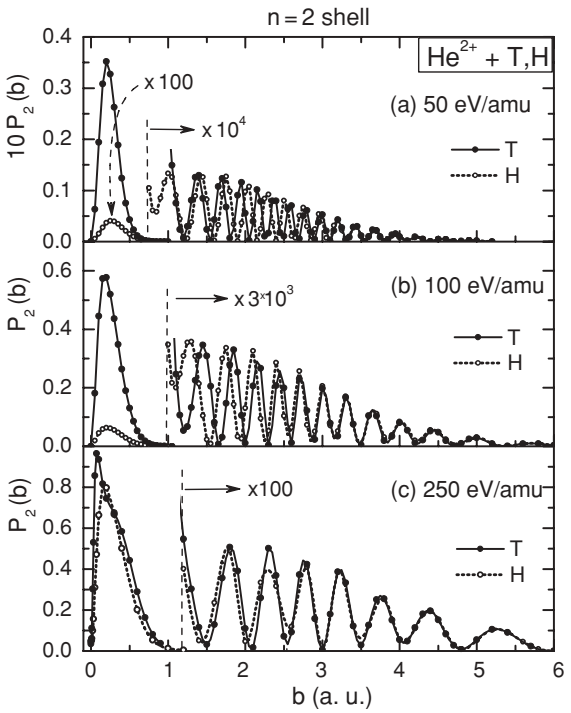

FIG. 3. Calculated probabilities $P_2(b)$ for charge exchange into the $n = 2$ shell in collisions of He^{2+} with H (dotted line) and T (solid line) as a function of the impact parameter b. The projectile energies are 50, 100, and 250 eV/amu as indicated in the graphs.

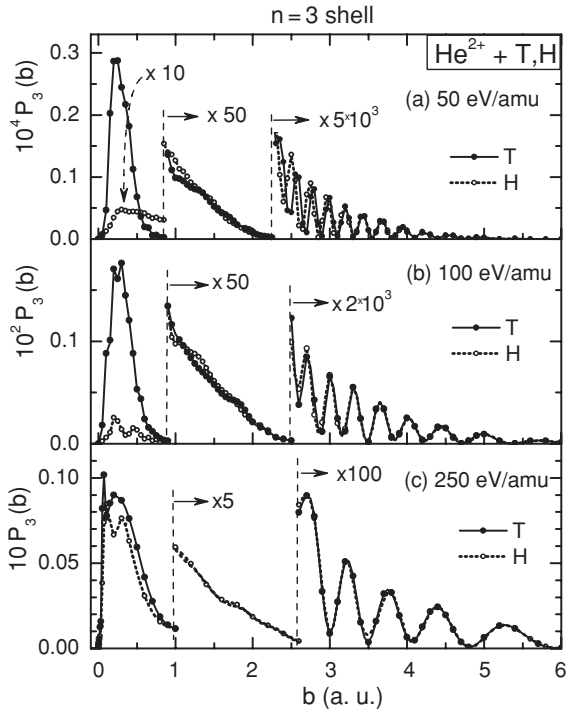

FIG. 4. Calculated probabilities $P_3(b)$ for charge exchange into the $n = 3$ shell in collisions of He^{2+} with H (dotted line) and T (solid line) as a function of the impact parameter b. The projectile energies are 50, 100, and 250 eV/amu as indicated in the graphs.

orbitals. At impact parameters larger than 1 a.u., $2p\sigma$-$3d\sigma$ radial coupling becomes dominant. In the range from 1 to 2.5 a.u. transitions due to the $2p\sigma$-$3d\sigma$ coupling mechanism are primarily followed by the sequence $3d\sigma$-$3d\pi$-$3d\delta$ of rotational couplings. In this range from 1 to 2.5 a.u. striking differences between capture into the $n = 2$ and that into the $n = 3$ shell are found. The Stueckelberg oscillations are missing due to negligible interferences in the pathway feeding the $n = 3$ shell, as discussed in detail in Ref. [18].

At larger impact parameters, $b > 2.5$ a.u., the $2p\sigma$-$3d\sigma$ transitions are predominantly followed by radial coupling of the $3d\sigma$-$4f\sigma$ orbitals. In that range oscillatory structures are observed. Comparison of Figs. 3 and 4 shows that the maxima and minima for the charge transfer probabilities into $n = 2$ and $n = 3$ occur at exactly the same positions. This is plausible, since the $n = 3$ population is preceded by the charge transfer into the $n = 2$ shell.

Similarly as for the $n = 2$ shell, the charge transfer into the $n = 3$ shell essentially agrees for the H and T isotopes within the outer region with $b = 1$–6 a.u. (Fig. 4). However, significant differences are observed within the inner region with $b < 1$ a.u., which is governed by rotational coupling mechanism. This provides evidence that the $2p\sigma$-$2p\pi$ rotational coupling is also responsible for the isotope effects on the charge transfer into the $n = 3$ shell. Again, the difference in the results for H versus T increases with decreasing energy, although the corresponding differences in the charge transfer into $n = 3$ are not as large as for $n = 2$.

Finally, we turn to the charge transfer into the $n = 1$ shell. Figure 5 displays probabilities $P_1(b)$ for that shell of He^{2+} in collisions with the isotopes H and T. For charge transfer into the $n = 1$ shell, we primarily consider the radial coupling of the $2p\sigma$ orbital with the $1s\sigma$ orbital, which correlates with the $1s$ state of the projectile [24,25]. A further pathway may be due to the rotational coupling sequence $2p\sigma$-$2p\pi$-$1s\sigma$. For 50 and 250 eV/amu the sharp peaks at small impact parameters are tentatively attributed to this rotational coupling sequence.

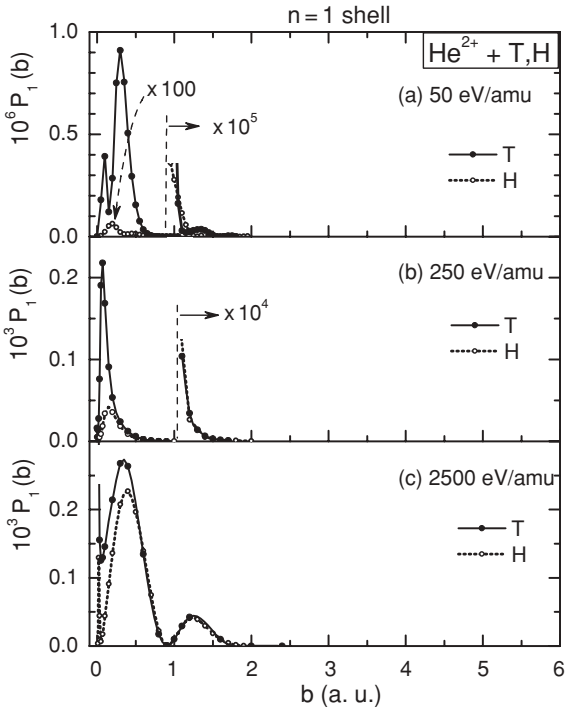

FIG. 5. Calculated probabilities $P_1(b)$ for charge exchange into the $n = 1$ shell in collisions of He^{2+} with H (dotted line) and T (solid line) as a function of the impact parameter b. The projectile energies are 50, 250, and 2500 eV/amu as indicated in the graphs.

For higher energies, 2500 eV/amu, the $2p\sigma$-$1s\sigma$ radial coupling localized near 1.4 a.u. gains importance. The peak at the impact parameter of 1.2 a.u. and the prominent maximum at 0.4 a.u. are likely be produced by this radial coupling (Fig. 5). Here, Stueckelberg oscillations may be present, similarly to the case of the $n = 2$ shell. Accordingly, for 2500 eV/amu a relatively small isotope effect is observed. However, at lower collision energies, significant differences between H and T occur within the inner region of $b < 1$ a.u. Also, these differences increase with decreasing energy. These findings are discussed in more detail in the following sections.

V. CHARGE TRANSFER CROSS SECTIONS

A. Total cross sections

In Fig. 6(a) the total cross sections for charge transfer are presented as a function of the energy of the He^{2+} impacting on H, D, and T. The data are obtained by integration of the corresponding capture probabilities including all shells. The present cross sections for H agree well with the results of Krstić *et al.* [8] and Le *et al.* [14]. The latter data sets typically deviate by 5% so they are presented here by a single solid line. The good agreement between the present results and those in Refs. [8] and [14] has been pointed out in I. It should be recalled, however, that the present data for the H target were obtained with a larger basis set, confirming their convergence, and also extended to lower energies (40 eV/amu).

Figure 6(a) shows that the cross sections for the different isotopes are nearly equal for energies $\gtrsim$300 eV/amu, whereas significant deviations are observed at lower energies. These deviations are more clearly revealed by the cross-section ratios for the isotopes T to H and D to H shown in Fig. 6(b). At energies of about 40–50 eV/amu the cross section increases dramatically, by orders of magnitudes, with an increase in the isotope mass. This finding is explained by the influence of the $2p\sigma$-$2p\pi$ rotational coupling mechanism as found in I and discussed previously here for the transfer probabilities. Moreover, it is pointed out that the extension of the present calculations indicates that the isotope effects reach a maximum near 40 eV/amu and start to decrease with decreasing projectile energy. Evidently, near this energy the rotational coupling contribution is maximal.

To reveal the magnitude of this rotational coupling, we evaluated the contribution of the radial coupling of the molecular orbitals $2p\sigma$ and $3d\sigma$. As described in I, we integrated the charge transfer probability in the outer region of $b > 1$ a.u. of the impact parameter, where the radial coupling dominates. Furthermore, we used the Stueckelberg formalism to estimate the radial coupling contribution into the inner region of $b < 1$ a.u. In Fig. 6(a) the contributions caused exclusively by radial coupling are depicted as triangles labeled "Rad." Furthermore, as described in I, we interpolated these END results by analytical calculations [28], which are referred

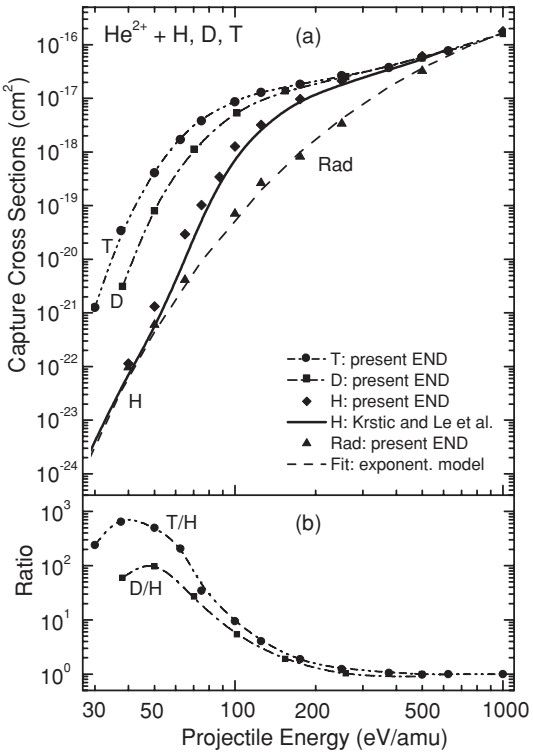

FIG. 6. (a) END results for charge exchange cross sections in collisions of He^{2+} with H (diamonds), D (squares), and T (circles) as a function of the projectile energy. The solid line represents the combined results of Krstić *et al.* [8] and Le *et al.* [14]. The dashed curve and the triangles are estimates of the radial coupling contribution. (b) Cross-section ratios T to H (T/H; circles) and D to H (D/H; squares). Data are plotted as a function of the reduced projectile energy ε_p.

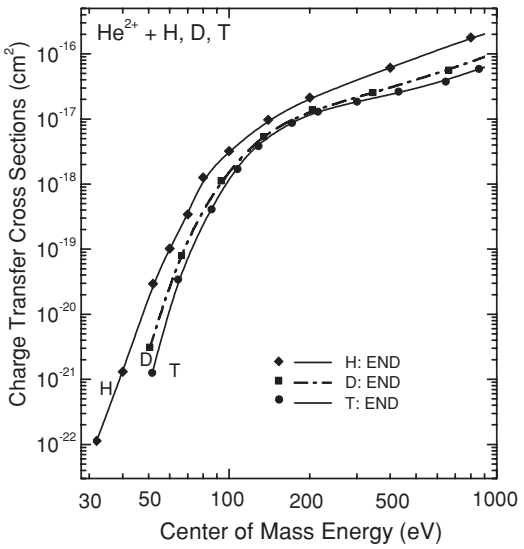

FIG. 7. Charge exchange cross sections in collisions of He^{2+} with H (diamonds), D (squares), and T (circles) as a function of the center-of-mass energy $E_p^{\text{c.m.}}$.

to as the exponential model and are given by the dashed curve in Fig. 6(a). As shown in the previous subsection, the isotope effects have only a minor influence on the radial coupling cross section. Therefore, within the present impact energy range the radial coupling contributions are essentially the same for H, D, and T. This is due to the fact that the radial coupling contribution is governed by the relative collision velocity, and hence, it scales with the laboratory energy of the projectile [see Eq. (2)].

For low collision energies, the recoiling target atom limits the distance of closest approach, R_{min}, between the collisions partners so that the rotational coupling region can no longer be reached. In particular, the distances of closest approach for H, D, and T differ significantly. It follows from Eq. (3) that at 100 eV/amu the distances of closest approach amount to $R_{\text{min}} = 0.65$, 0.4, and 0.3 a.u., respectively, for impact parameters close to zero. Thus, the rotational coupling region is accessed more with increasing mass of the isotopes. Accordingly, at 100 eV/amu the cross section for T is an order of magnitude larger than that for H (Fig. 6).

The results for R_{min} from Eq. (3) suggest a scaling of the charge transfer cross sections in terms of the center-of-mass energy. Indeed, as shown in Fig. 7 the differences among the results for H, D, and T are reduced when the total cross sections are plotted as a function of $E_p^{\text{c.m.}}$. However, significant deviations remain in the cross sections of the isotopes. In the energy region near 60 eV, where the rotational coupling dominates, the cross sections of H and T differ by a factor of ~5 (see also in I). Furthermore, at the high energy limit, where the radial coupling dominates, the cross sections do not merge together. Moreover, at the low-energy limit, the cross sections exhibit deviation as high as a factor of 20. These deviations at the low and high energies can be understood from the fact that the radial coupling scales with the relative velocity and, thus, with the reduced laboratory energy ε_p, so that differences are produced when the data are plotted as a function of $E_p^{\text{c.m.}}$. Therefore, in the following, we continue to display the results for the cross sections as a function of ε_p as is common use in atomic collision physics.

B. Shell-selective cross sections

In the following, we discuss the charge transfer into individual shells of the projectile. Figure 8 shows the shell-selected cross sections for the transfer of an electron from atomic hydrogen H into the $n = 1$, 2, and 3 shells of He^{2+}. It is evident that the cross sections for the $n = 2$ shell are dominant. The cross sections for $n = 3$ and 2 differ by a factor of 10–100, whereas the cross sections for $n = 1$ are smaller than those for $n = 2$ by several orders of magnitude. The dominance of the cross sections for the $n = 2$ shell relative to the $n = 3$ shell can be understood from the discussion of the corresponding probabilities in the previous section. For energies higher than 5 keV/amu the data sets for $n = 2$ and 3 deviate from those by Minami *et al.* [13] by a factor of up to 1.5. This may be due partially to the opening of the ionization channel, which is not properly described in the END approach. However, we point out for these energies up to 10 keV/amu that the total cross sections (sum over $n = 1$–3) agree well with the data of Minami *et al.* [13] and the recommended values [7].

In the energy range from 1000 eV/amu upward the cross sections for $n = 1$ exhibit a strong quasiexponential

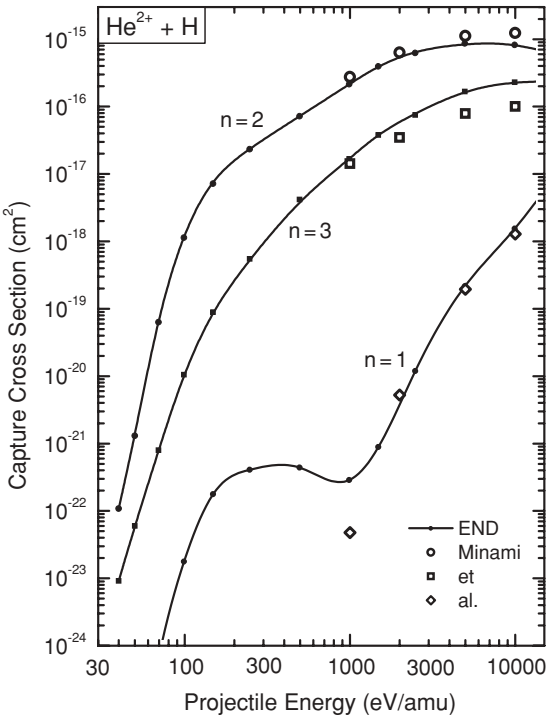

FIG. 8. Shell-selective cross sections for charge transfer from atomic hydrogen H into the shells of principal quantum number $n = 1$, 2, and 3 of He^{2+}. Results displayed as open circles, squares, and diamonds are taken from Minami *et al.* [13].

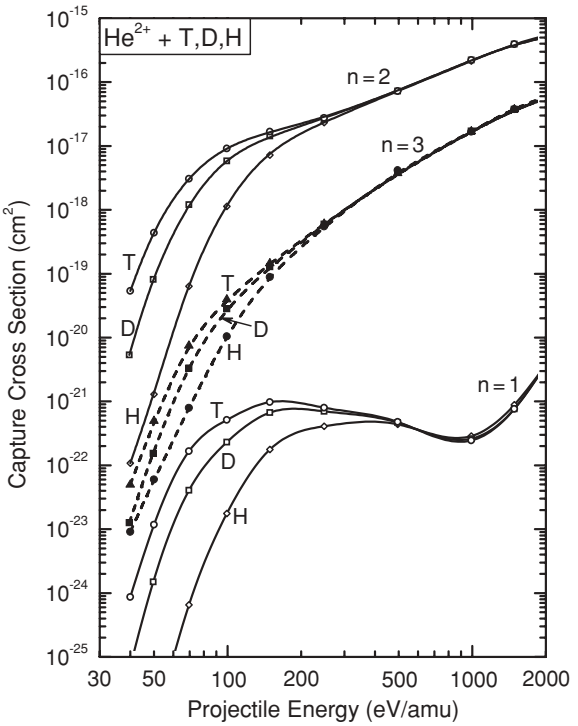

FIG. 9. Shell-selective cross sections for collisions of He^{2+} with H, D, and T as a function of the projectile energy. Data are given for the $n = 1$, 2, and 3 shells, as indicated on the curves.

increase with the projectile energy, which is typical for the radial coupling mechanism [28]. Hence, at energies above 1000 eV/amu, radial coupling is expected to be dominant. At lower energies a hump structure is observed with a maximum at about 300 eV/amu. This structure may be due to the rising influence of the rotational coupling sequence $2p\sigma$-$p\pi$-$1s\sigma$. In Fig. 8 we observe excellent agreement with previous data of Minami *et al.* [13] except for the data point at 1000 eV/amu. It is noted that the calculations of Minami *et al.* [13] are performed with straight-line trajectories, which may influence the low-energy data. However, we suggest that further studies are needed to verify the hump structure in conjunction with the discrepancy at 1000 eV/amu.

To demonstrate the isotope effects on the shell-selective cross sections, the results for the different target atoms are compared in Fig. 9. It is shown that these effects differ for different shells. The visibility of the isotope effects is enhanced in Fig. 10, where the cross-section ratios for D and H (left) and for T and H (right) are plotted. As expected the isotope effects for the T-H cross-section ratio exceed those of the corresponding D-H results. In Fig. 10 each panel incudes data for the individual shells $n = 1$, 2, and 3. The isotope effects for the $n = 2$ shell are similar to those for the total cross section shown in Fig. 6(b).

This is plausible, since the total cross sections are dominated by the charge transfer into the $n = 2$ shell. The isotope effects for the $n = 3$ shell is significantly smaller than those for the $n = 2$ shell. The corresponding cross-section ratios do not exceed a factor of 10. The largest isotope effects are found for the $n = 1$ shell.

To interpret the isotope effects for the different shells, it is recalled that they are mainly produced by rotational coupling mechanisms. Thus, the differences in the shell-selective cross sections can be associated with the radii of the rotational coupling regions feeding the different shells. The rotational coupling $2p$-$2p\pi$, relevant for the $n = 2$ shell, occurs at distances of the order of 1 a.u. and less. The populations of $n = 1$ and 3 shells start with the same rotational coupling. However, these populations require additional couplings, which may alter somewhat the position of the coupling regions. As discussed before, the isotope effects are governed by the

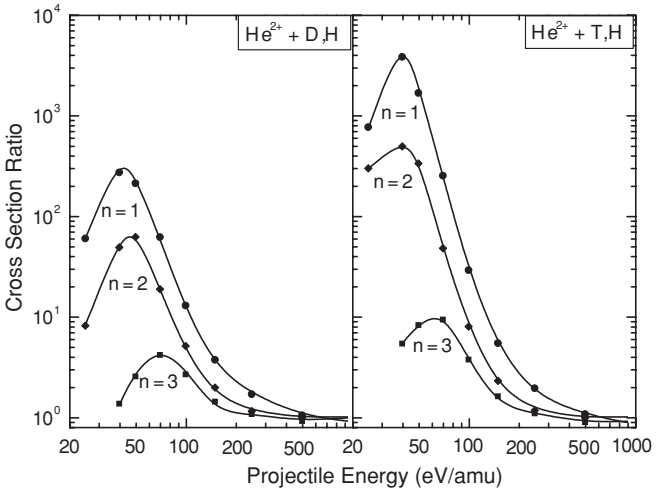

FIG. 10. Shell-selective cross-section ratios D to H (left) and T to H (right). Data are based on results shown in Fig. 9.

distance of closest approach of the collision particles in relation to the coupling radius relevant for the charge transfer. Hence, we may understand that the isotope effects exhibit differences, since the corresponding coupling regions differ in position.

VI. CONCLUSIONS

In conclusion, we have calculated charge transfer probabilities and cross sections for collision systems, which are of considerable importance for fundamental theoretical developments. Furthermore, the present results are expected to be important for applications such as modeling specific processes in fusion reactors and astrophysical phenomena. In comparison with I, the charge transfer probabilities and cross sections have been recalculated with an extended basis set to minimize convergence problems at low collision energies.

At larger impact parameters, the charge transfer probabilities exhibit well-known Stueckelberg oscillations which are produced by the coherent contributions from two localized coupling regions, which suggests similarities to Young's two-slit experiment. The specific property of the present case is that the distance between the transition regions ("slits") is of atomic dimension.

At smaller impact parameters the charge transfer probabilities show enormous isotope effects, which increase with decreasing projectile energy. In the region of small impact parameters, rotational coupling is responsible for the charge transfer, whereas at higher impact parameters radial coupling is dominant. Thus, the rotational and radial coupling contributions can be well separated. In particular, this separation unambiguously reveals that the isotope effects in the present collision systems are essentially produced by rotational coupling mechanisms.

The isotope effects are visible also in the total cross sections, for which the different contributions due to radial and rotational coupling were evaluated. The radial couplings are shown to be nearly equal for all isotopes. However, the rotational coupling contributions for the different isotopes are found to differ by orders of magnitude. The analysis of the distance of closest approach suggests scaling the cross section by the center-of-mass energy. However, it is shown that significant isotope effects remain when such scaling is performed. This finding is due to the radial coupling contribution to the total cross section, which scales with the laboratory energy, so that it should not be plotted as a function of the center-of-mass energy.

Particular attention is given to isotope effects on the cross sections for the individual shells. Since the charge transfer into the $n = 2$ shell is dominant, the isotope effects associated with this shell are similar to those for the total cross section. However, isotope effects for the $n = 1$ and 3 shells are found to be significantly different from those for $n = 2$. The strong shell dependence of the isotope effect is attributed to differences in the positions of the coupling regions.

ACKNOWLEDGMENTS

The University of Florida High Performance Computing Center is acknowledged for providing computer resources and support. R.C.-T acknowledges support from Grant No. PAPIIT-UNAM 107108 and the CONACyT-SNI consolidation program under Grant No. 089607. P.K. acknowledges support from the US DOE Office of Fusion Sciences through ORNL, under Contract No. DE-AC05-00OR22725 with UT-Battelle, LLC. The work was also supported by NSF Grant No. 00057476 to Y.Ö. and E.D.

[1] B. H. Bransden and M. R. C. McDowell, *Charge Exchange and the Theory of Ion-Atom Collisions* (Clarendon Press, Oxford, 1992).
[2] V. A. Krasnopolsky, M. J. Mumma, M. Abbott, B. C. Flynn, K. J. Meech, D. K. Yeomans, P. Feldman, and C. Cosmovici, Science **277**, 1488 (1997).
[3] D. Bodewits, Z. Juhász, R. Hoekstra, and A. G. G. M. Tielens, Astrophys. J. Lett. **606**, L81 (2000).
[4] D. Bodewits, R. Hoekstra, B. Seredyuk, R. W. McCullough, G. H. Jones, and A. G. G. M. Tielens, Astrophys. J. Lett. **642**, 593 (2006).
[5] R. K. Janev and J. J. Smith, At. Mol. Phys. **117**, 83 (1991).
[6] R. K. Janev, *Atomic and Molecular Processes in Fusion Edge Plasmas* (Plenum, New York, 1995).
[7] R. Hoekstra, D. Bodewits, S. Knoop, R. Morgenstern, L. Méndez, L. F. Errea, C. Illescas, A. Macías, B. Pons, A. Riera, F. Aumayr, and H. Winter, At. Plasma-Matter Interact. Data Fusion **13**, 8 (2007).
[8] P. S. Krstić, J. Phys. B **37**, L217 (2004).
[9] C. C. Havener, R. Rejoub, P. S. Krstić, and A. C. H. Smith, Phys. Rev. A **71**, 042707 (2005).
[10] R. Hoekstra, A. R. Schlatmann, F. J. de Heer, and R. Morgenstern, J. Phys. B **22**, L603 (1989).
[11] E. A. Solov'ev, Sov. Phys. Usp. **32**, 228 (1989).
[12] R. K. Janev and J. J. Smith, Material Interaction Data for Fusion **4**, 1 (1993).
[13] T. Minami, T. G. Lee, M. S. Pinzola, and D. R. Schultz, J. Phys. B **41**, 135201 (2008).
[14] A. T. Le, C. D. Lin, L. F. Errea, L. Méndez, A. Riera, and B. Pons, Phys. Rev. A **69**, 062703 (2004).
[15] N. Stolterfoht, R. Cabrera-Trujillo, Y. Öhrn, E. Deumens, R. Hoekstra, and J. R. Sabin, Phys. Rev. Lett. **99**, 103201 (2007).
[16] E. C. G. Stueckelberg, Helv. Phys. Acta **5**, 369 (1932).
[17] T. Young, *A Course of Lectures on Natural Philosophy and the Mechanical Arts* (Johnson, London, 1807).
[18] N. Stolterfoht, R. Cabrera-Trujillo, P. S. Kristić, Y. Öhrn, E. Deumens, and R. Sabin, Int. J. Quantum Chem. **109**, 3063 (2009).
[19] E. Deumens, A. Diz, R. Longo, and Y. Öhrn, Rev. Mod. Phys. **66**, 917 (1994).
[20] R. Cabrera-Trujillo, J. R. Sabin, E. Deumens, and Y. Öhrn, Adv. Quantum Chem. **48**, 47 (2005).
[21] R. Cabrera-Trujillo, J. R. Sabin, E. Deumens, and Y. Öhrn, Phys. Rev. A **71**, 044702 (2005).
[22] R. Cabrera-Trujillo, E. Deumens, Y. Öhrn, O. Quinet, J. R. Sabin, and N. Stolterfoht, Phys. Rev. A **75**, 052702 (2007).

[23] T. H. Dunning Jr., J. Chem. Phys. **90**, 1007 (1989).
[24] T. P. Grozdanov and E. A. Solov'ev, Phys. Rev. A **42**, 2703 (1990).
[25] P. S. Krstić and R. K. Janev, Phys. Rev. A **47**, 3894 (1993).
[26] K. Taulbjerg, J. S. Briggs, and J. Vaaben, J. Phys. B **9**, 1351 (1976).
[27] T. P. Grozdanov and E. A. Solov'ev, J. Phys. B **15**, 3871 (1982).
[28] Y. N. Demkov, Zh. Eksp. Teor. Fiz. **49**, 195 (1963).
[29] This is illustrated in Fig. 5 of Ref. [8], which compares the fully quantum treatment of the internuclear motion with Coulomb trajectory calculations previously performed by T. G. Winter and N. F. Lane, Phys. Rev. A **17**, 66 (1978).